AIMS Materials Science, 13(1): 99–119.
DOI: 10.3934/matersci.2026006
Received: 11 November 2025
Revised: 26 November 2025
Accepted: 05 December 2025
Published: 22 January 2026

https://www.aimspress.com/journal/Materials

Research article

Extraction of chitosan-based piezoelectric thin film from shrimp shell waste

Firzanah Hisham[1], Kartini Ahmad[1,*], Maziati Akmal Mohd Hatta[1] and Farah Ahmad[2]

[1] Department of Science in Engineering, Kulliyyah of Engineering, International Islamic University Malaysia, 53100 Gombak, Selangor, Malaysia
[2] Department of Chemical Engineering and Sustainability, Kulliyyah of Engineering, International Islamic University Malaysia, 53100 Gombak, Selangor, Malaysia

* **Correspondence:** Email: kartini@iium.edu.my; Tel: +603-6196-6528; Fax: +603-6421-6594.

Abstract: In this study, we explored the potential of chitosan, a natural polysaccharide derived from shrimp shell waste, for piezoelectric applications in biomedical, food, and agricultural industries. Despite limited research on its piezoelectric properties, chitosan has gained attention due to its non-toxicity and energy-harvesting potential. We focused on optimizing the extraction of chitosan from shrimp shell waste for these applications. Chitin powder was treated with NaOH concentrations ranging from 30% to 60% to remove acetyl groups and create chitosan. The best results for chitosan extraction were achieved using a 50% NaOH solution. Piezoelectric properties of chitosan thin films dissolved in formic acid were also analyzed, showing the best performance with a piezoelectric constant (k) of 0.3158, maximum charge (Q_m) of 64.1, and a low loss tangent ($tan\ \delta$) of 0.0156. Later, the biological assessment of the chitosan thin films, namely the antimicrobial and biocompatibility analyses, were performed to evaluate their interaction with biological systems and to determine their potential for biomedical and biotechnological applications. The results indicated that the chitosan thin film exhibited no cytotoxic effects, highlighting its promise as a safe and suitable material for diverse biomedical uses.

Keywords: extraction; chitosan; shrimp shell; piezoelectric; thin film

1. Introduction

Concerns regarding energy sources that can give unlimited power without endangering nature or the environment have been raised by the rise in integrated and miniaturised smart and electronic devices on the Internet of Things (IoT) [1]. Electrochemical batteries were used in the past to power the electrical devices. Notably, electrochemical batteries have a limited lifespan, cause an adverse effect on the environment, and require maintenance [2]. On the other hand, harvesting ambient sources of energy like heat, mechanical vibrations, electromagnetic radiation, and fluid flows can provide clean and viable energy for various electronic gadgets like portable electronics, wireless sensor networks, wearables, and implantable biomedical tools [3]. Of all the available renewable energies, mechanical energy would be the most suitable for self-powered items because of its availability and environmental viability. Numerous ambient sources, including wind, vibration, sound waves, and human body movement, can possess mechanical energy [4]. Among other technologies, like electromagnetic, thermoelectric, and electrostatic, piezoelectric material-based technology, also known as piezoelectricity, is the best and most viable for infinite self-powered tools [5,6]. This is because it makes use of a particular material with inherent piezoelectricity to produce electricity when subjected to ambient vibration.

Piezoelectric materials have the capacity to generate mechanical movement or vibration or an electrical potential in reaction to an applied force. The capacity to generate piezoelectricity, ease of obtaining the source [7], and biocompatibility [8] are essential when choosing piezoelectric material from natural sources. Currently, traditional piezoelectric material encompasses 2 polymer-based polyvinylidene fluoride (PVDF) and ceramic-based lead zirconium titanate (PZT). These materials not only have a high piezoelectric coefficient but also superior mechanical strength and the benefit of a steady and noticeable piezoelectric impact [9]. These two materials do, however, have some drawbacks: the use of piezoelectric ceramics, such as PZT, in smart biomedical devices is constrained by their typical fragility and substandard biocompatibility [10]. According to Ibn-Mohammed et al., lead oxide (PbO) discharges from PZT-based products could happen in several ways, such as evaporation during calcination and sintering at extreme temperatures [11]. This is one more problem with typical piezoelectric materials. The use of PZT may be extremely dangerous due to the lead discharge and its toxicity, which may be made worse by the volatilization at extreme temperatures during sintering and calcination [12]. Because of its greater acoustic impedance, the presence of lead results in a very high density, a property that may provide a significant obstacle in actuator and sensor applications. Conversely, when exposed to a very alkaline environment, the synthetic piezoelectric polymer known as PVDF tends to breakdown. Nonetheless, PVDF continues to be an unsuitable material in terms of ecological and biological contexts. Thus, PZT and PVDF are inappropriate for use as piezoelectric materials from the point of view of biomedicine, such as tissue engineering [13].

It is critical to choose piezoelectric materials carefully because improper human use might create biocompatibility and toxicity issues, leading to adverse health and environmental outcomes. Here, we assess several materials for piezoelectric instruments. Observations indicate the biological substances might have piezoelectric properties like synthetic substances. Considering the crystallinity and non-toxic nature, the bio-polymer chitosan is a potent eco-friendly piezoelectric material for energy extraction. Reports suggest that the concurrent use of chitosan and collagen polymers produces a noteworthy rise in the piezoelectric strain constant (d_{33}) [14]. Studies concerning chitosan structure indicated the presence of dipolar alignments and constricted charges owing to the electronegativity of

nitrogen, leading to a lasting dipole moment, producing electricity in a unit cell structure. The presence of a net dipole moment and changes in electronegativity values are vital for determining cell polarisation, highlighting the piezoelectric abilities of the material [15].

Chitosan is produced because of the deacetylation of chitin obtained from shrimp shells, which are the most common commercial raw material for chitin production. It is estimated that nature contains about 100 billion tonnes of chitin [16]. Considering the use of discarded shrimp shells, using shrimp-based chitosan for piezoelectric materials is eco-friendly. For example, the local areas have ramped up cultured shrimp production, leading to higher shrimp shell biowaste in Malaysia [17,18]. It is estimated that 45% of such processed foods ends up in landfills, leading to foul odors and aesthetic impacts on nature [19,20].

Despite the fact that chitosan extraction from shrimp shell waste is well-documented, researchers who develop and evaluate shrimp-shell-derived chitosan thin films for targeted piezoelectric applications remain limited. For instance, Kota et al. (2023) focus on chitosan production or biomedical applications rather than dedicated piezoelectric device development. Amran et al. (2021) investigated piezoelectric behaviour, but it used microbial chitosan rather than chitosan produced from shrimp shell waste [21,22]. Moreover, chitosan-based piezo electrics have been rare since the twenty-first century because practical outcomes indicate 0.1 to 2 pC/N levels, which are technologically inadequate for gathering energy [23]. The piezoelectric properties of chitosan are not fully established; hence, it is challenging to enhance piezoelectric sensitivity. A detailed assessment of the biological, electrical, and structural characteristics must be conducted to use this biomaterial as a reliable energy harvesting source, like manufactured polymers.

2. Materials and methods

2.1. Materials

Shrimp shell waste was collected from local fish sellers. Pristine chemicals were used for evaluation. Sigma Aldrich provided NaOH pellets (98%), while R&M Chemicals provided hydrochloric acid (37%).

2.2. Extraction of chitin and chitosan

The shell waste was washed and oven-dried at 65 ºC for 4 days. It was then crushed into a powder and placed in a closed container.

2.2.1. Deproteinisation

The shrimp shell powder was treated with 1 M NaOH. This alkaline process used a 1:5 (w/v) solid-to-solvent ratio. This experiment required 20 h at room temperature (28 ± 2 ºC). The remains were then washed using distilled water to neutralise the chemicals.

2.2.2. Demineralisation

Different HCl concentrations (1%, 2%, 3%, 4% and 5%) were used to trigger demineralisation. This treatment required 16 h and was conducted at room temperature (28 ± 2 ºC) at a 1:5 (w/v) solid-to-solvent ratio. The remains were then filtered, rinsed, and soaked in distilled water to obtain a neutral pH level. The produced residue at this stage was called chitin.

2.2.3. Deacetylation

Concentrated NaOH (50% (w/v)) was used on chitin to eliminate the acetyl group and produce chitosan. A 20 h treatment was provided at 65 ºC at a 1:10 (w/v) solid-to-solvent ratio. Subsequently, the samples were rinsed until the sample had a neutral pH. The chitosan was then dried for 4 h at 65 ºC.

2.3. Fabrication of chitosan thin film

A total of 0.5 g finely ground chitosan was mixed in 2% acid solution to produce a chitosan thin film. Formic, lactic, acetic, tartaric, and citric acids were used to produce this thin film. The chemicals were stirred thoroughly and mixed at 1000 rpm for 3 h at 60 ºC. Subsequently, 20 mL of this material was placed on a petri dish, which was stored in a dry place for 5 h at 55 ºC.

2.4. Characterisation

2.4.1. Crystalline structure

X-ray diffraction (XRD) assessment of the chitosan sample was performed at 2θ = 5–40º. A Bruker D2 Phaser was set at 40 kV and 40 mA voltage and current levels for processing chitosan. A thin-film-specific machine (PANalytical model X'Pert3 Powder) was used for XRD assessment of thin films. The crystallinity index (CrI%) was then computed using Eq 1 [22]:

$$\mathrm{CrI\%} = \left(\frac{I_{110} - I_{am}}{I_{110}}\right) \times 100\% \quad (1)$$

where I_{110} is the maximum intensity of the (110) diffraction peak in the crystalline region at 20º and I_{am} is the highest intensity of amorphous diffraction at 16º.

2.4.2. Fourier-transform infrared spectroscopy (FTIR)

The obtained chitin and chitosan were evaluated for chemical structure based on the FTIR model Nicolet iS50. FTIR characteristics were obtained in the central infrared (4000 to 400 cm^{-1}) region at 2 cm^{-1} resolution. The degree of deacetylation (DDA) can be computed based on Eq 2 [22]:

$$\mathrm{DDA} = 97.67 - 26.486 \times \left(\frac{A_{1655}}{A_{3450}}\right) \quad (2)$$

where A_{1655} and A_{3450} are the absorbance band at 1655 and 3450 cm^{-1}, respectively.

2.4.3. Field emission scanning electron microscopy (FESEM)

The thin films of the two materials were assessed for morphology using FESEM (JEOL JSM-700F) images. Every sample was sputter coated with gold to reduce charging levels.

2.4.4. Piezoelectric properties' measurement

Solarton Analytical (model 1280C) electromechanical test setup was used (Figure 1) to ascertain the electrical characteristics of the chitosan thin film. This device provides the electromechanical coupling factor (k), quality factor value (Q_m), and dissipation factor ($tan\ \delta$) pertaining to the chitosan thin film voltage and frequency ranges were set at 0.001 to 10 kV and 1 Hz to 1 MHz, respectively.

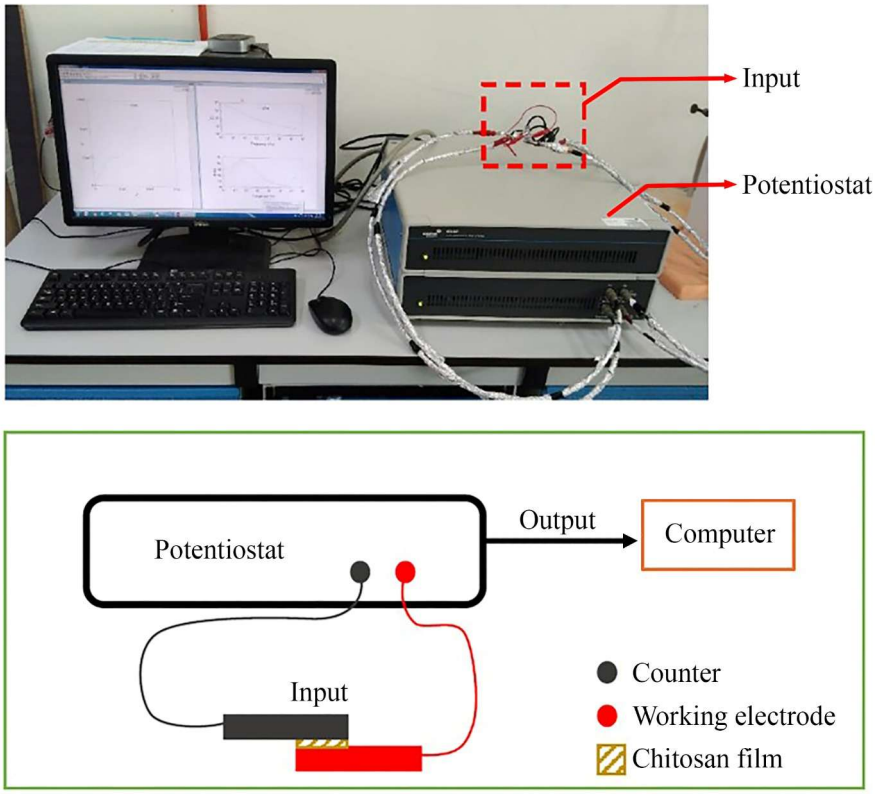

Figure 1. Experimental setup for piezoelectric property measurement of chitosan thin film using it as a high-performance electrochemical impedance analyzer and its schematic drawing.

2.4.5. Antimicrobial test

Tryptic Soy Broth (TSB) was placed on a petri dish. The assessment was conducted using an agar medium. Adequate dilution levels were obtained, followed by *Escherichia coli* (ATCC 8739) and *Staphylococcus aureus* (ATCC 25923) inoculation. A 1.5 cm diameter film was sliced and put on the inoculated culture surface. Bacterial growth was stimulated by maintaining the dish between 32–37 ºC. After one day, the film's inhibition region was assessed to evaluate if bacterial growth was impacted.

2.4.6. Biocompatibility test

Cellular metabolic characteristics were evaluated using the 3-(4,5-dimethylthiazol-2-yl)-2,5-diphenyl-2H-tetrazolium bromide (MTT) assay to understand cell viability, proliferation, and cytotoxicity. Considering that pre-clinical evaluations are necessary to ascertain material and instrument biocompatibility, such assays are critical for dentistry-specific medical equipment and material. An L-929 was used to assess the dose-specific cytotoxicity [23]. A 2 mg/mL growth medium was used to treat the chitosan thin film, followed by 0.2 μm membrane processing for sterilisation. Sequential two-fold dilution was achieved pertaining to the complete growth medium before cellular exposure. Cellular exposure was made at chitosan concentrations of 0.063, 0.125, 0.25, 0.5, 1, and 2 mg/mL of the chitosan thin film for 24 h. Tetrazolium salts (MTT) were used to assess cytotoxicity and cell viability. The cell viability was attained using Eq 3:

$$\text{Cell viability} = \frac{\text{The mean of optical density (OD)}}{\text{The mean OD of negative control}} \times 100\% \quad (3)$$

3. Results

3.1. Extraction of chitosan from shrimp shell waste

Shrimp-based chitin and chitosan were evaluated for functional groups, surface morphology, and crystallinity.

3.1.1. Crystallinity of chitin and chitosan from shrimp shells

XRD has been employed for analysis of the crystalline structure pertaining to the pure shrimp shells as well as the extracted chitin. With regards to the pure shrimp shells and chitin samples, prominent peaks were seen near $2\theta = 20°$ and $2\theta = 10°$ as well as diffracted at planes (110) and (020), respectively (Figure 2). The amide II ($–NH_2$) plane is represented by (110) plane, while the amide I ($–N–CO–CH_3$) plane by the (020) plane [24]. This suggests that an α-chitin crystalline structure was included in both materials. At the centre of these structures, there is a lack of symmetry which results in the creation of dipole moments (μ), thereby inducing piezoelectricity. Since the peak almost disappeared at the (020) plane, low crystallinity was observed in the pure shrimp shell sample. However, after extraction of the chitin, the peaks were seen to become narrower at planes (110) and (020). This suggests that the crystallinity pertaining to the α-chitin structure would get enhanced after the elimination step of calcium carbonate ($CaCO_3$) in the demineralisation process [25]. Thus, increased crystallinity indicates successful removal of $CaCO_3$ and proteins from the pure shrimp shells.

To further analyse deacetylated chitosan caused by changing concentrations of NaOH, XRD was employed. The XRD analysis established that the pronounced peaks occurred around $2\theta = 10°$ and $2\theta = 20°$. When increasing the NaOH concentration to 50%, the peaks were observed to be intensified. In all the chitosan samples, a high degree of crystallinity was confirmed based on the intense peaks observed at planes (020) and (110), which are due to enhanced extra-molecular and inter-molecular hydrogen bonding after deacetylation [26]. However, when increasing the NaOH concentration to 60%, broadening of both peaks were seen, denoting a decrease in crystallinity. This could be due to the generation of high alkaline concentration (NaOH) during the deacetylation process,

leading to disruption of the order of macromolecule and polymer chain of heterogeneity, thereby causing distortion of the crystalline structure in the chitosan sample [27].

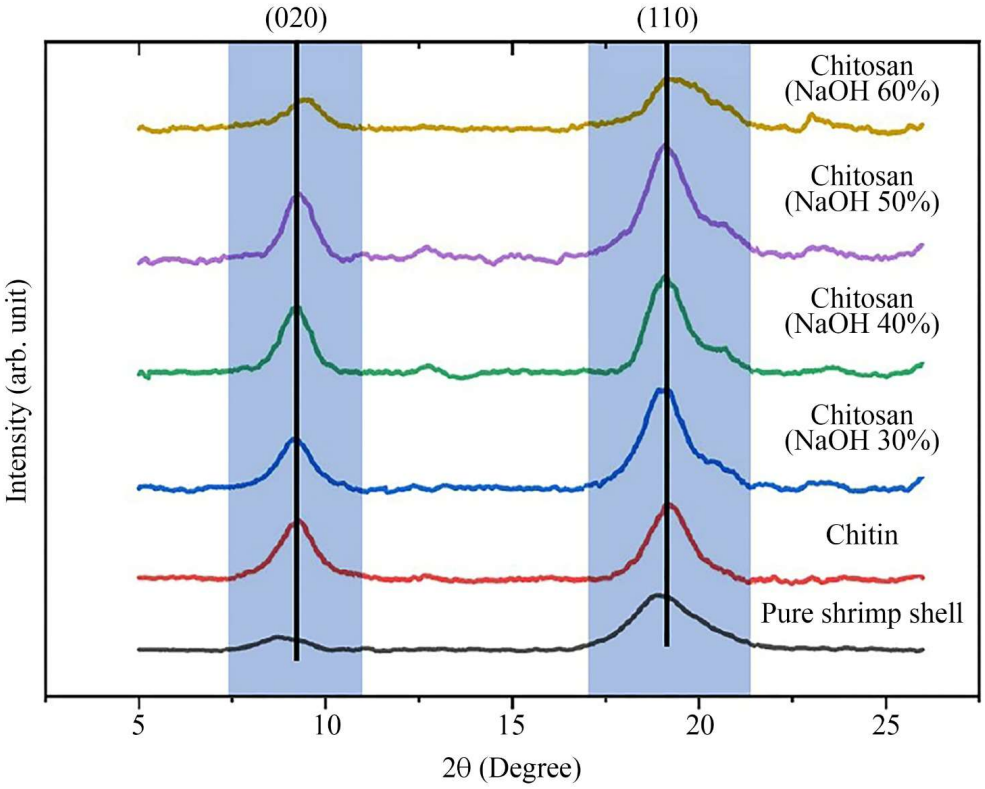

Figure 2. The XRD results of pure shrimp shells, chitin, and chitosan deacetylated with varying NaOH concentrations.

Calculation of the CrI% was done, representing perfect, ordered, and average crystallite sizes [28]. It was seen that the CrI% of the chitin and the chitosan had an impact on their biological and physical characteristics, mostly biodegradability and solubility. As observed in Figure 3, higher CrI% (81.5%) was seen with chitin versus pure shrimp shells (60.2%). However, there were minor variations observed in CrI% of the 30%, 40%, and 50% NaOH-chitosan samples, while the 60% NaOH-chitosan sample yielded a CrI% of 60.3%, which was almost similar when compared with the pure shrimp shells.

As mentioned, a higher CrI% (81.5%) was associated with the chitin versus chitosan. Similarly, as per Ahmad et al. [27], chitin displayed considerably more crystalline characteristic versus chitosan [29]. The associated comparatively low CrI% and the formation of amorphous structures could be due to the breakdown of the inter-molecular and intra-molecular hydrogen bonds with regards to the 60% NaOH-chitosan sample. Moreover, increasing the extent of deacetylation as well as exposing chitosan to extreme reaction conditions can decrease and degrade by the crystallinity pertaining to chitosan [30]. In contrast, 50% NaOH provided high purity and minimal structural compromise, making it the most optimum condition overall.

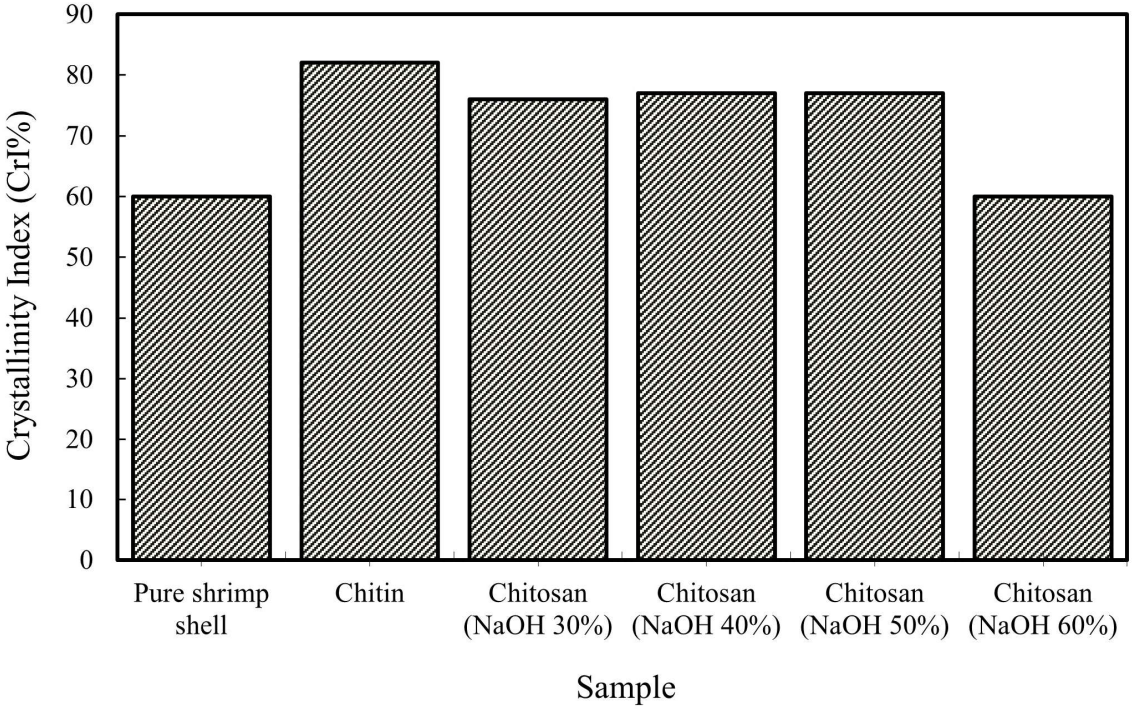

Figure 3. The CrI% of chitosan deacetylated with varying NaOH concentrations.

3.1.2. Functional groups of chitin and chitosan derived from shrimp shell waste

The FTIR spectra pertaining to the pure shrimp shells and the chitin is displayed in Figure 4. The optimised chitin showed visible absorption bands. The extraction of chitin from the pure shrimp shells is represented by the presence of two separate peaks at 1656 and 1625 cm^{-1} bands, corresponding to the stretching vibration band regarding the amide I region [31]. The XRD result was also supported by the α-chitin isomorph characteristic. Apart from that, a distinctive stretching vibration that is found in the amide II region was observed at the 1553 cm^{-1} band [32]. Moreover, at bands 3436 and 3256 cm^{-1}, O–H and N–H stretching vibrations could be observed, respectively. At 1376 cm^{-1}, a peak was seen and was recognised as a C–H bond, which was identical to the appearance pertaining to the primary peaks in the extracted chitin's FTIR spectra [16].

Figure 4 also includes the FTIR spectra pertaining to the chitosan deacetylated by employing different concentrations of NaOH. At 1655 and 1620 cm^{-1}, considerable changes could be seen, wherein the amide I band had weakened on deacetylation of the chitosan with 60% NaOH. Fundamentally, both bands are key as they confirm that the amide I band is present and helps to identify the kind of chitin polymorphic conformations [33]. According to other researchers, the polymer chain degradation was observed when studying the deacetylation process, despite the use of longer treatment durations and higher concentrations of alkaline, as supported by their findings [34]. Thus, for the deacetylation process, 60% NaOH was regarded to be unsuitable as there was a chance that the chitosan structure could get damaged.

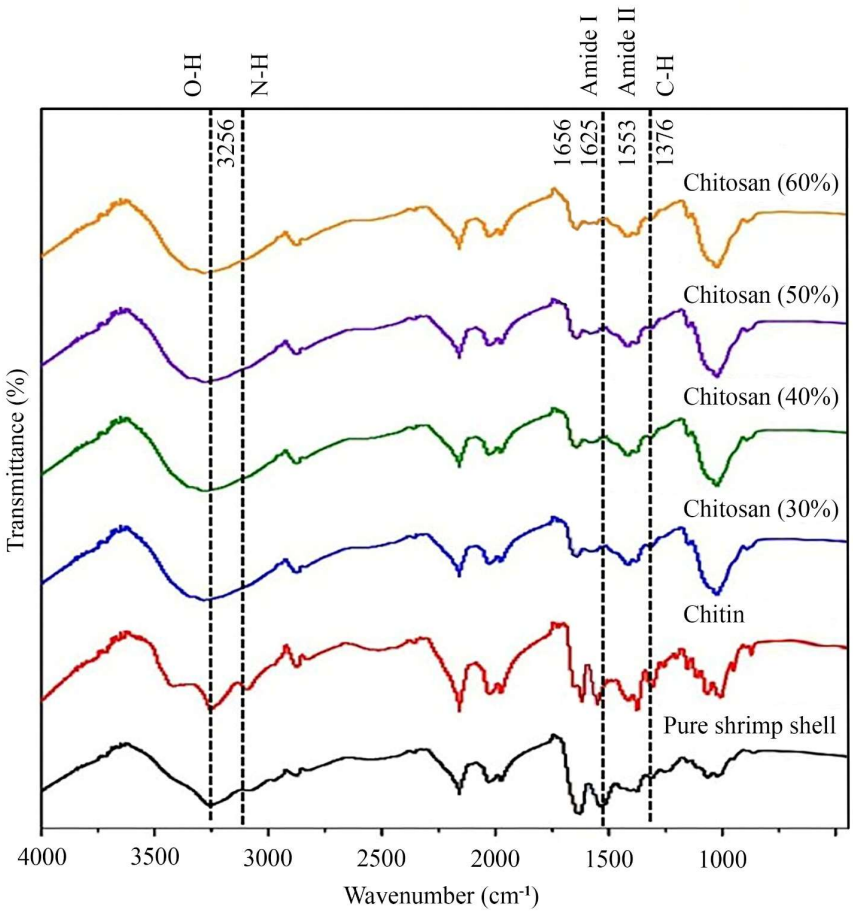

Figure 4. The FTIR spectra of the pure shrimp shells and the chitin as well as the 30%, 40%, 50%, and 60%-NaOH-chitosan samples.

By eliminating the acetyl group from chitin, chitin is converted to chitosan via the deacetylation process [35]. However, the DDA determines the efficiency pertaining to the conversion of chitin to chitosan. Thus, the DDA of the chitosan deacetylated with different NaOH concentrations was calculated by employing the FTIR spectra results. As observed in Figure 5, when there was increase in NaOH concentration, the DDA was also seen to increase. The highest DDA (74.6%) was seen with the 50% NaOH-chitosan sample, indicating that 74.6% of the acetyl group was eliminated from the acetamide group (–$NHCOCH_3$) and that the chitin was successfully converted into chitosan [36]. DDA is regarded as crucial for maintaining highly soluble characteristics of chitosan when placed in the appropriate solvent for subsequent thin film fabrication because of the removal of the acetyl group. Conversely, when there was an increase in the concentration of NaOH to 60%, the DDA was seen to decrease to 65.3%. This may have been caused by the presence of high concentration of NaOH, which can degrade the polymer chain in the deacetylation process [37].

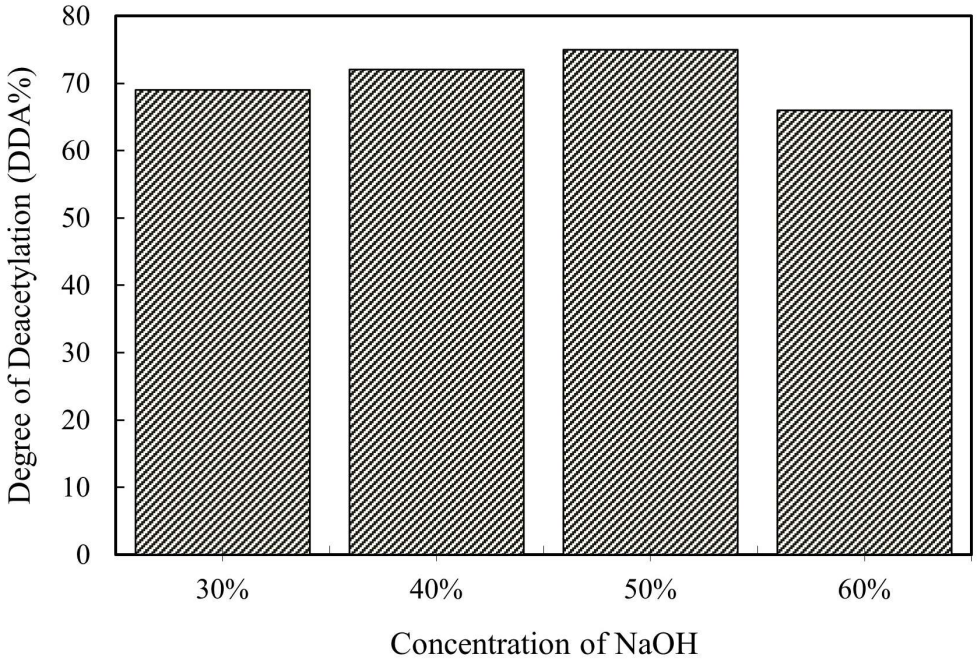

Figure 5. The DDA of the 30%, 40%, 50%, and 60%-NaOH-chitosan samples.

3.1.3. Surface morphology of chitin and chitosan

The surface morphology pertaining to the pure shrimp shells and the chitin was assessed by employing field emission scanning electron microscopy (FESEM). Because of the presence of proteins and minerals, the pure shrimp shells were seen to possess an uneven and rough surface (Figure 6a), which was almost the same as that of Andrade et al. [37]. However, a uniform and homogenous structure was seen with the chitin (Figure 6b). This was possible because of the deproteinization and demineralisation processes, which enabled removing minerals and proteins from the pure shrimp shells, thereby enhancing the chitin structure's densification [38].

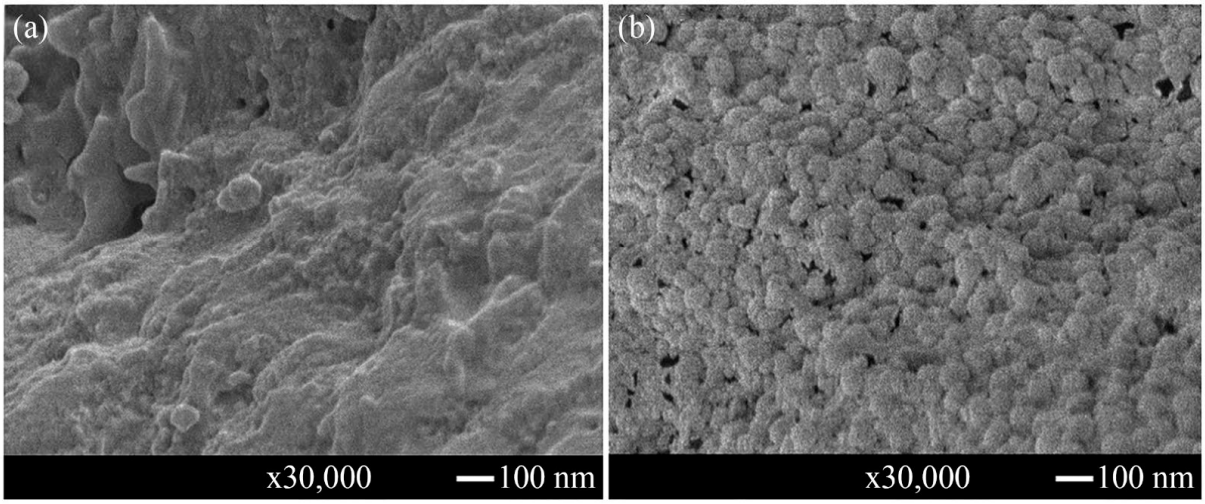

Figure 6. Morphology of the (a) pure shrimp shells and (b) chitin.

Figure 7 shows the chitosan's surface morphology exposed to different NaOH concentrations. A coarse surface along with irregular-shaped aggregates was associated with 30% NaOH-chitosan sample (Figure 7a), while a surface that was rough but agglomerated was seen with the 40% NaOH-chitosan sample (Figure 7b). The 50% NaOH-chitosan sample demonstrated smoother morphology with pores absent (Figure 7c), hinting towards a near complete deacetylation of chitosan [39]. However, the surface pertaining to the 60% NaOH-chitosan sample was seen to be coarse along with visible pores (Figure 7d). This was due to the chitosan structure getting damaged with high NaOH concentrations [36].

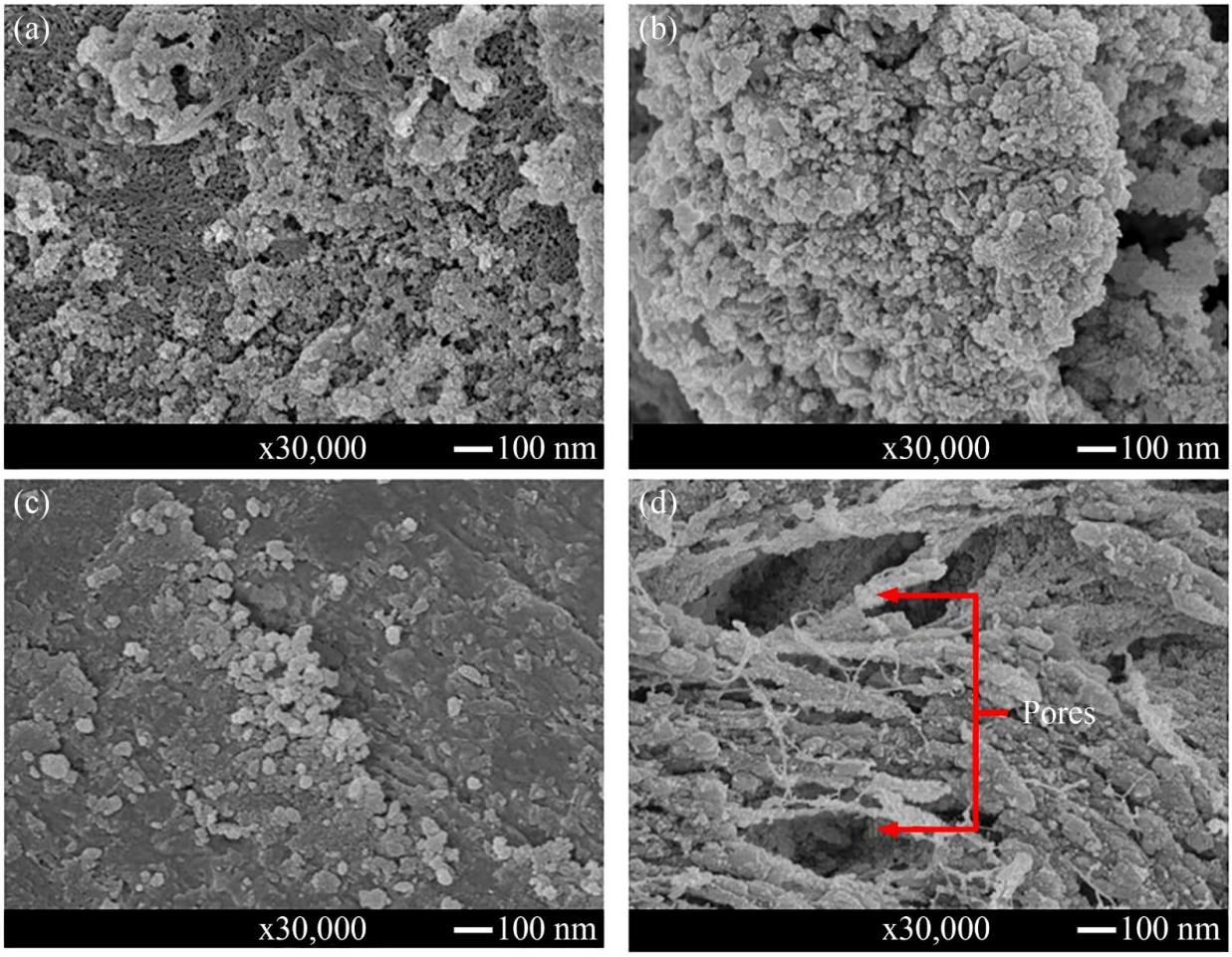

Figure 7. The morphology of the (a) 30%, (b) 40%, (c) 50%, and (d) 60% NaOH-chitosan.

3.2. Fabrication of chitosan thin film via solvent casting

Chitosan is regarded as the only commercially available water-soluble cationic biopolymer that can dissolve in diluted acid solutions (pH > 6.5) while not dissolving in alkaline or neutral aqueous solutions [40]. To fabricate thin films, it is important that chitosan remains dissolved in the acid. Thus, the type of acid employed plays an important role regarding the dissolution of chitosan. The current study also evaluated the efficacy of employing formic acid, acetic acid, citric acid, lactic acid, and tartaric acid to produce chitosan thin films (CTFs). For this study, these acids were shortlisted since they are di-functional carboxylic acids, which aids in dissolving chitosan as well as the ionic crosslinks

of its chains to fabricate flexible CTFs [41]. As per the results described in Section 3.1, selection of the 50% NaOH-chitosan powder sample was done with regards to CTF fabrication because of its high DDA, highly crystalline structure, and its smooth surface, since these characteristics promote good solubility in acid solvents, a characteristic key to fabricating flexible CTFs.

3.2.1. Crystallinity of chitosan thin films

XRD was employed to examine the CTFs crystallinity (Figure 8). As seen, each of the CTFs had a similar orientation that was like planes (020) and (110) [42]. Those peaks developed around $2\theta = 10°$ and $2\theta = 20°$. This indicated that the primary peaks noted in the films were obtained from the chitosan powder sample's peaks. Notably, the shift of the small peak could be because of diverse matrix interactions such as the acid proton's interaction with the nitrogen atom of chitosan's amine group, inter-molecular restructuring, and changes in principal chain alignment [43]. Of the five films, the citric acid-CTF intensity at plane (020) seemed to almost disappear. As per Qiao et al., strong intermolecular associations between the citric acid and the chitosan inhibit the chain segments from movement, therefore inhibiting the process of crystallisation [44].

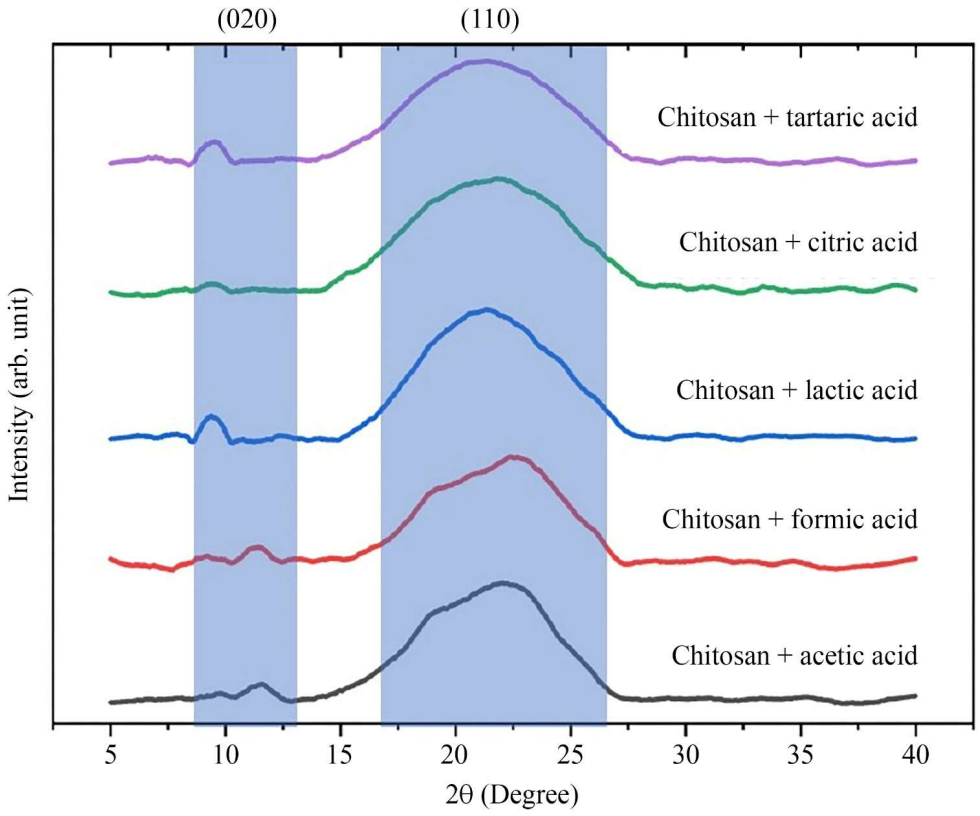

Figure 8. The XRD results of CTFs dissolved in different types of acids.

As displayed in Figure 9, the formic acid-CTF had the maximum CrI% (92%) followed by lactic acid, acetic acid, citric acid, and tartaric acid, in descending order. With respect to piezoelectricity, a CrI% increase could improve the piezoelectric constant. As enhanced crystallite restructuring and crystallinity lead to a larger total dipole moment, it generates a bigger piezoelectric coefficient [45].

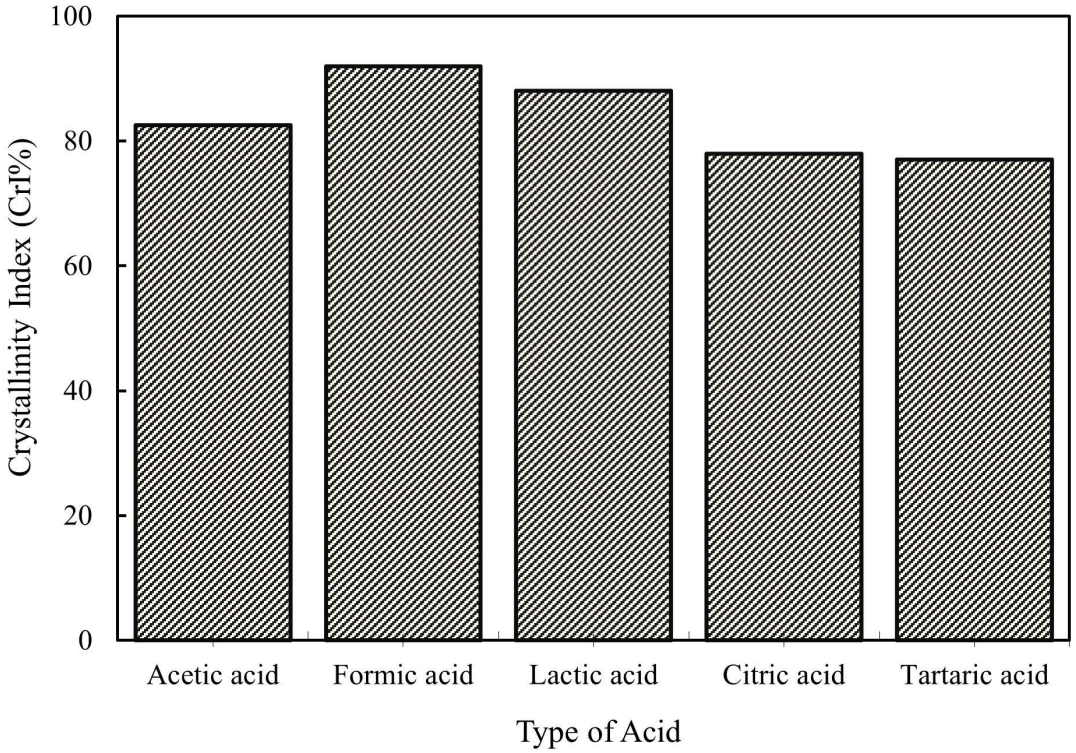

Figure 9. The CrI% of CTFs dissolved in different types of acids.

3.2.2. Morphology of chitosan thin films

Figure 10 displays the CTF surface morphology at a 30k magnification. Substantial cracks were seen in the tartaric acid-, citric acid-, and lactic acid-CTFs, of which the largest cracks were observed in the tartaric acid-CTF. This may be because of relatively poor polymer chain configuration [46]. Conversely, the formic acid-CTF had a homogenous and even surface owing to better polymer chain packing between the formic acid and the chitosan. It is notable that the presence of cracks or apertures may obstruct the material's dipole movement and reduce the film's crystallinity, which reduces the piezoelectric effect.

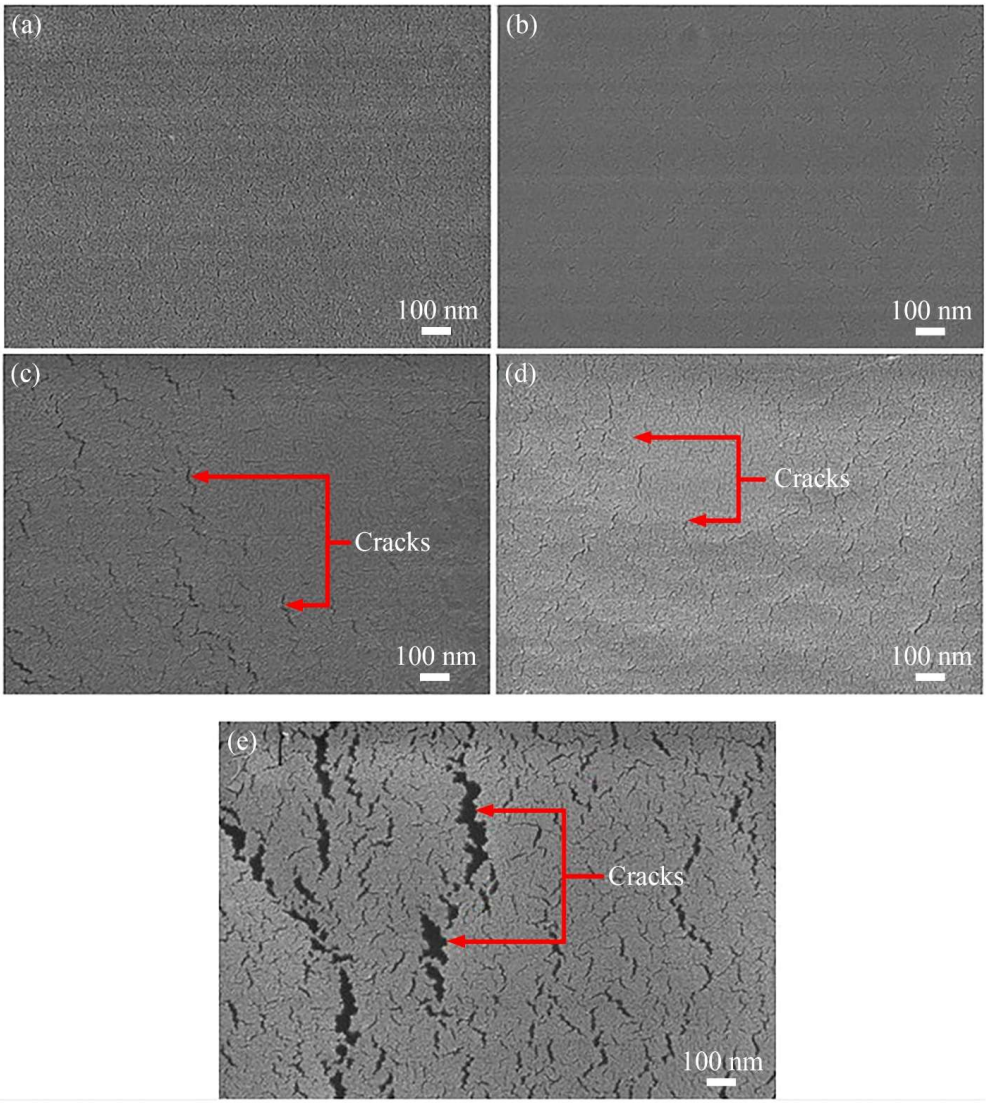

Figure 10. The surface morphology of CTFs dissolved in (a) acetic acid, (b) formic acid, (c) lactic acid, (d) citric acid, and (e) tartaric acid.

3.2.3. Piezoelectric properties of chitosan thin films

The mechanical quality parameter (Q_m) is the most significant extrinsic aspect in improvement of the piezoelectric response. Excellent piezoelectric materials are presumed to be having a high factor for mechanical quality (~20–300 for polymer) owing to their capability to increase the dipole moments' orientation which, accordingly, enhances the piezoelectric response within the crystal configuration [47]. Besides, the electromechanical coupling factor (k) represents a measure of the piezoelectric material ability to transform mechanical energy into electrical energy or vice versa. Thus, a higher k value (close to 1) is desirable. Hence, several critical electrical parameters, namely electromechanical coupling factor (k), quality factor (Q_m), and the dissipation factor ($tan\ \delta$), were examined to determine the piezoelectric characteristics of each CTF. These values were noted down at a 100 Hz resonance frequency.

Based on Figure 11, the formic acid-CTF sample exhibits the best piezoelectric properties, as evidenced by its highest Q_m (64) and piezoelectric coefficient k (0.31). This might be due to the formic

acid-CTF's high CrI%, which in turn, enhanced its crystallinity and densification. As an improvement in crystallinity enables dipole-dipole movement, it improved the formic acid-CTF's piezoelectric response [48]. Moreover, its high Q_m suggested that it was an excellent piezoelectric material since it could manage recurring mechanical vibrations under resonance. Interestingly, the k (31%) of the chitosan film of this research was much greater than those of Wittinanon, Rianyoi, and Chaipanich at 16.74% [49].

Figure 11 also shows the *tan* δ of the CTFs. The *tan* δ regulates the rate of loss of energy of the piezoelectric material. The *tan* δ was lowest (0.0156) for formic acid-CTF. This was likely because of an increase in local charge carriers, which decreased the *tan* δ within the chitosan's crystalline structure [50].

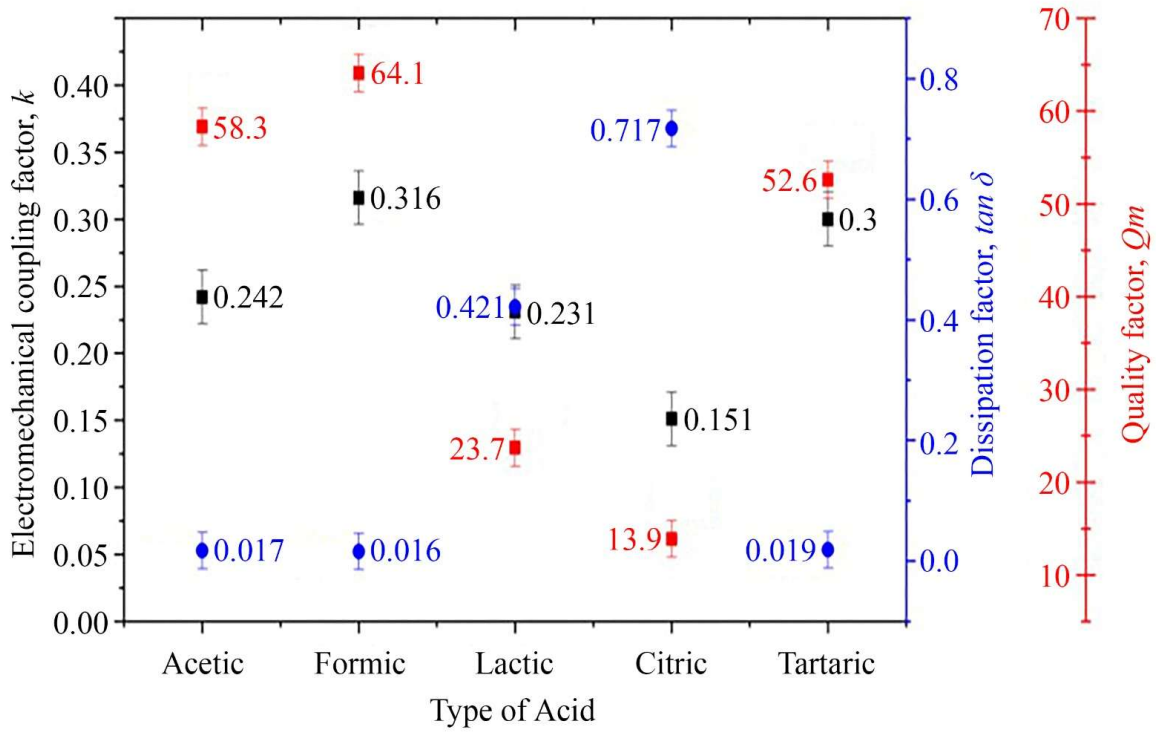

Figure 11. Quality factor (Q_m), electromechanical coupling factor (k), and the dissipation factor ($tan\ \delta$) of chitosan thin films dissolved in different types of acid solvents.

3.3. Biological assessment of the chitosan thin films

Predicated on the outcomes of the piezoelectric characteristics, crystallinity, tensile strength, and morphology evaluations, the formic acid-CTF produced the most excellent results. Thus, it was chosen for further biological evaluation in terms of biocompatibility and antibacterial properties.

3.3.1. Antimicrobial analysis of chitosan thin films

An antimicrobial examination was carried out to study the formic acid-CTF's resistance to pathogens. Two kinds of bacteria were used: (1) *Staphylococcus aureus* (*S. aureus*); a gram-positive strain, and (2) *Escherichia coli* (*E. coli*); a gram-negative strain. Notably, the observed clear area above the chitosan antibacterial zone in Figure 12a was due to the diffusion pattern of the extractant or

residual solvent when the sample was placed on the agar. This area did not represent additional antibacterial activity, but rather an artifact of uneven solvent diffusion or surface moisture during the assay. Figure 12b exhibits the formation of a prevention zone in the vicinity of the formic acid-CTF. The size of the inhibition size was indicated using Ampicillin. The inhibition zone was bigger in the *S. aureus* culture at 13 mm, whereas it was 11 mm for the *E. coli* culture. Other researchers observed that their chitosan solution developed inhibition zones of similar size of 10 mm in both *E. coli* and *S. aureus* cultures [51]. Thus, CTFs can effectively inhibit the progress of microorganisms, especially *S. aureus* and *E. coli.*

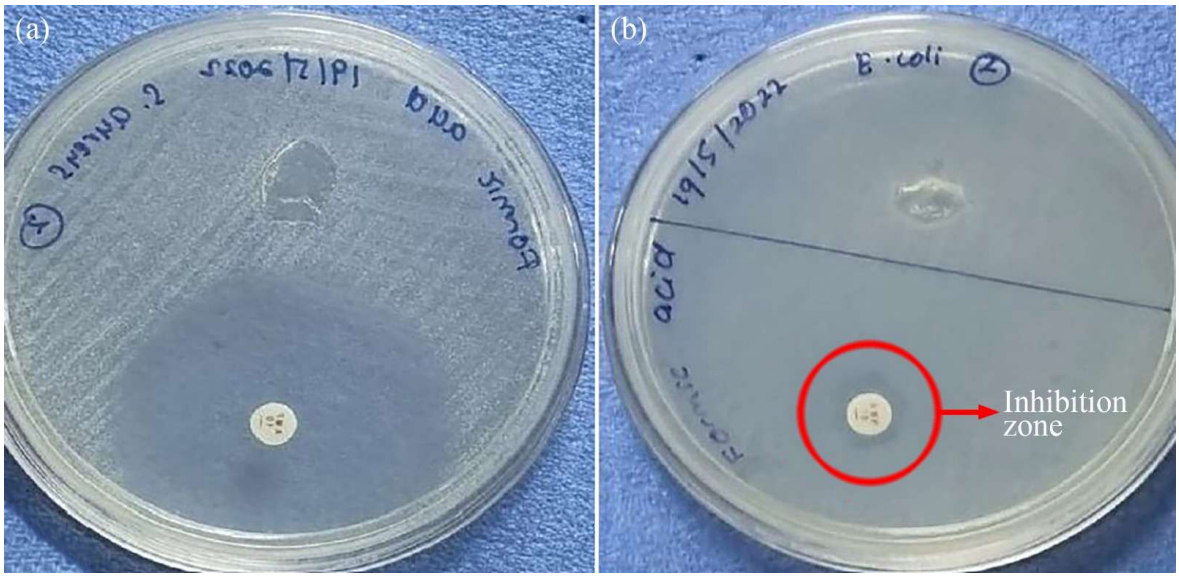

Figure 12. The inhibition zones surrounding formic acid-CTFs in (a) *S. aureus* and (b) *E. coli* cultures.

3.3.2. Biocompatibility analysis of chitosan thin films

The MTT test was performed to examine the formic acid-CTF's cytotoxicity. As per ISO 10993-5:2009 (E) guidelines, the formic acid-CTF was not cytotoxic since more than 70% of the L-929 cell remained workable after 24 h [52]. Figure 13 exhibits the L-929 cells' viability at different concentrations of the formic acid-CTF. As per the observation, even at the maximum concentration of 2mg/mL, it did not inhibit the L-929 cells viability by more than 30% after an exposure of 24 h. Therefore, chitosan thin film did not exhibit a cytotoxic effect under the study conditions.

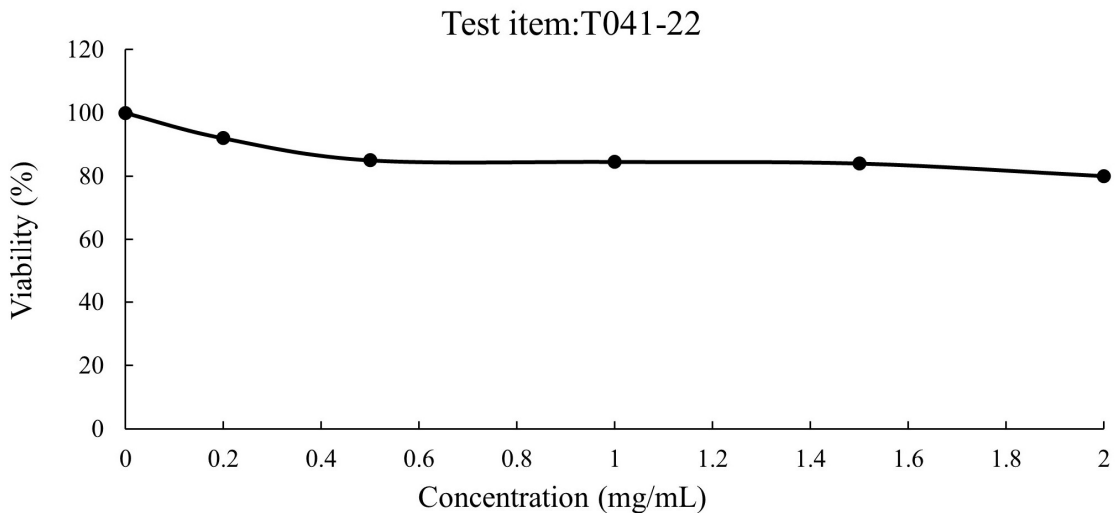

Figure 13. The viability of L-929 cells at various formic acid-CTF concentrations. "Test item: T041-22" refers to the sample identification code assigned by the biocompatibility testing laboratory.

4. Conclusions

To conclude, 50% was the best NaOH concentration for extracting chitosan from clean shrimp shells, whereas formic acid was the best suited acid for CTF formation since it produced a material with excellent piezoelectric characteristics. The XRD examination demonstrated that the formic acid-CTF possessed the maximum CrI% (92%), whereas its electrical characteristics (k = 0.316, Q_m = 64.1, and $tan\ \delta$ = 0.421) were the most suitable for a piezoelectric material. Furthermore, the antimicrobial assays revealed the development of inhibition zones measuring 11 and 13 mm around formic acid-CTFs in *E. coli* and *S. aureus* cultures, respectively. Finally, the cytotoxicity examination demonstrated that the formic acid-CTF did not impede the L-929 cell viability by more 30%. Hence, the formic acid-CTF was not cytotoxic and could be used in low-frequency piezoelectric applications. Moreover, it has potential as a biocompatible piezoelectric material for some applications as an alternative to traditional lead-containing materials.

Use of AI tools declaration

The authors declare they have not used Artificial Intelligence (AI) tools in the creation of this article.

Acknowledgments

The authors wish to express their gratitude for the financial support provided by the Ministry of Higher Education Malaysia through the Fundamental Research Grant Scheme (FRGS/1/2019/TK05/UIAM/02/7).

Author contributions

Firzanah Hisham: conceptualization, data curation, investigation, writing–original draft; Kartini Ahmad: supervision, writing, review & editing; Maziati Akmal Mohd Hatta: supervision, formal analysis, data validation; Farah Ahmad: supervision, data validation.

Conflict of interest

The authors declare no conflict of interest.

References

1. Padhy A, Joshi S, Bitragunta S, et al. (2021) A survey of energy and spectrum harvesting technologies and protocols for next generation wireless networks. *IEEE Access* 9: 1737–1769. https://doi.org/10.1109/ACCESS.2020.3046770
2. Mishu MK, Rokonuzzaman M, Pasupuleti J, et al. (2020) Prospective efficient ambient energy harvesting sources for IoT-equipped sensor applications. *Electronics* 9: 1345. https://doi.org/10.3390/electronics9091345
3. Sezer N, Koç M (2021) A comprehensive review on the state-of-the-art of piezoelectric energy harvesting. *Nano Energy* 80: 105567. https://doi.org/10.1016/j.nanoen.2020.105567
4. Wu CX, Kima TW, Sung S, et al. (2017) Ultrasoft and cuttable paper-based triboelectric nanogenerators for mechanical energy harvesting. *Nano Energy* 44: 279–287. https://doi.org/10.1016/j.nanoen.2017.11.080
5. Ahmad MM, Khan FU (2021) Review of vibration-based electromagnetic–piezoelectric hybrid energy harvesters. *Int J Energy Res* 45: 5058–5097. https://doi.org/10.1002/er.6253
6. Kumar S, Singh HH, Khare N (2019) Flexible hybrid piezoelectric-thermoelectric generator for harnessing electrical energy from mechanical and thermal energy. *Energ Convers Manage* 198: 111783. https://doi.org/10.1016/j.enconman.2019.111783
7. d'Angelo M, Benedetti E, Tupone MG, et al. (2019) The role of stiffness in cell reprogramming: a potential role for biomaterials in inducing tissue regeneration. *Cells* 8: 1036. https://doi.org/10.3390/cells8091036
8. Chorsi MT, Curry EJ, Chorsi HT, et al. (2019) Piezoelectric biomaterials for sensors and actuators. *Adv Mat* 31: 1802084. https://doi.org/10.1002/adma.201802084
9. Wankhade SH, Tiwari S, Gaur A, et al. (2020) PVDF–PZT nanohybrid based nanogenerator for energy harvesting applications. *Energy Rep* 6: 358–364. https://doi.org/10.1016/j.egyr.2020.02.003
10. Yuan H, Lei T, Qin Y, et al. (2019) Design and application of piezoelectric biomaterials. *J Phy D: App Phy* 52: 194002. https://doi.org/10.1088/1361-6463/ab0532
11. Ibn-Mohammed T, Reaney IM, Koh SCL, et al. (2018) Life cycle assessment and environmental profile evaluation of lead-free piezoelectrics in comparison with lead zirconate titanate. *J Europ Ceramic Soc* 38: 4922–4938. https://doi.org/10.1016/j.jeurceramsoc.2018.06.044
12. Jain A, Prashanth KJ, Sharma AK, et al. (2015) Dielectric and piezoelectric properties of PVDF/PZT composites: A review. *Poly Eng Sci* 55: 1589–1616. https://doi.org/10.1002/pen.24088

13. Jacob J, More N, Kalia K, et al. (2018) Piezoelectric smart biomaterials for bone and cartilage tissue engineering. *Inflam Regener* 38: 1–11. https://doi.org/10.1186/s41232-018-0059-8
14. Hänninen A, Sarlin E, Lyyra I, et al. (2018) Nanocellulose and chitosan-based films as low cost, green piezoelectric materials. *Carbohydr Polym* 202: 418–424. https://doi.org/10.1016/j.carbpol.2018.09.001
15. Ghasemian MB, Daeneke T, Shahrbabaki Z, et al. (2020) Peculiar piezoelectricity of atomically thin planar structures. *Nanoscale* 12: 2875–2901. https://doi.org/10.1039/C9NR08063E
16. Al Shaqsi NHK, Al Hoqani HAS, Hossain MA, et al. (2020) Optimization of the demineralization process for the extraction of chitin from Omani Portunidae segnis. *Biochem Biophy Rep* 23: 100779. https://doi.org/10.1016/j.bbrep.2020.100779
17. Tan JS, Abbasiliasi S, Lee CK, et al. (2020) Chitin extraction from shrimp wastes by single step fermentation with Lactobacillus acidophilus FTDC3871 using response surface methodology. *J Food Process Preserv* 44: e14895. https://doi.org/10.1111/jfpp.14895
18. Tan HW, Lim ZYJ, Muhamad NA, et al. (2022) Potential economic value of chitin and its derivatives as major biomaterials of seafood waste, with particular reference to southeast Asia. *J Renew Mat* 10: 909. https://doi.org/10.32604/jrm.2022.018183
19. Monjane J, Chemane D, Zimba A, et al. (2021) Production of chitosan from crab shells using an aqueous extract of wood ash for the deacetylation of chitin: An innovative, eco-friendly, and low-cost method. *Am J Polym Sci Technol* 7: 29–37. https://doi.org/10.11648/j.ajpst.20210702.12
20. Owuamanam S, Cree D (2020) Progress of bio-calcium carbonate waste eggshell and seashell fillers in polymer composites: A review. *J Compos Sci* 4: 70. https://doi.org/10.3390/jcs4020070
21. Kota S, Anantha R, Govada VR, et al. (2023) Chitosan/PVA films and silver nanoparticle impregnated nanofibrous dressings for evaluation of their wound healing efficacy in Wistar Albino rat model. *J Polym Mat* 40: 285–303. https://doi.org/10.32381/JPM.2023.40.3-4.10
22. Amran A, Ahmad FB, Akmal MHM, et al. (2021) Biosynthesis of thin film derived from microbial chitosan for piezoelectric application. *Mater Today Comm* 29: 10291. https://doi.org/10.1016/j.mtcomm.2021.102919
23. Fukada E (2000) History and recent progress in piezoelectric polymers. *IEEE T Ultrason Ferr* 47: 1277–1290. https://doi/org/10.1109/58.883516
24. Vicente FA, Huš M, Likozar B, et al. (2021) Chitin deacetylation using deep eutectic solvents: ab initio-supported process optimization. *ACS Sust Chem Eng* 9: 3874–3886. https://dx.doi.org/10.1021/acssuschemeng.0c08976
25. Zhao D, Huang WC, Guo N, et al. (2019) Two-step separation of chitin from shrimp shells using citric acid and deep eutectic solvents with the assistance of microwave. *Polymers* 11: 409. https://doi.org/10.3390/polym11030409
26. Rizwan M, Yahya R, Hassan A, et al. (2018) Synthesis of a novel organosoluble, biocompatible, and antibacterial chitosan derivative for biomedical applications. *J App Polym Sci* 135: 45905. https://doi.org/10.1002/app.45905
27. Ahmad LO, Permana D, Wahab Sabarwati, et al. (2015) Improved chitosan production from tiger shrimp shell waste (Penaeus monodon) by multistage deacetylation method and effect of bleaching. *Adv Environ Geol Sci Eng* 373–378.
28. Sa Y, Guo Y, Feng X, et al. (2017) Are different crystallinity-index-calculating methods of hydroxyapatite efficient and consistent? *New J Chem* 41: 5723–5731. https://doi.org/10.1039/C7NJ00803A

29. Aboudamia FZ, Kharroubi M, Neffa M, et al. (2020) Potential of discarded sardine scales (Sardina pilchardus) as chitosan sources. *J Air Waste Manage Assoc* 70: 1186–1197. https://doi.org/10.1080/10962247.2020.1813840
30. Amoo KO, Olafadehan OA, Ajayi TO (2019) Optimization studies of chitin and chitosan production from Penaeus notialis shell waste. *Afri J Biotech* 18: 670–688. https://doi.org/10.5897/AJB2019.16861
31. Liu Y, Xing R, Yang H, et al. (2020) Chitin extraction from shrimp (Litopenaeus vannamei) shells by successive two-step fermentation with Lactobacillus rhamnoides and Bacillus amyloliquefaciens. *Int J Biologic Macromolecules* 148: 424–433. https://doi.org/10.1016/j.ijbiomac.2020.01.124
32. Zidani J, Zannen M, Da Costa A, et al. (2024) Investigation of microstructure and physical characteristics of eco-friendly piezoelectric composite thin films based on chitosan and Ln_2O_3-doped $Na_{0.5}Bi_{0.5}TiO_3$–$BaTiO_3$ nanoparticles. *Nanomaterials* 14: 1755. https//doi.org/10.3390/nano14211755
33. Hahn T, Tafi E, Paul A, et al. (2020) Current state of chitin purification and chitosan production from insects. *J Chem Tech Biotech* 95: 2775–2795. https://doi.org/10.1002/jctb.6533
34. Ahing FA, Wid N (2016) Extraction and characterization of chitosan from shrimp shell waste in Sabah. *Trans Sci Tech* 3: 227–237.
35. Elsabee MZ, Morsi RE, Fathy M (2020) Chemical modifications of chitin and chitosan, In: Kim SK, *Encyclopedia of Marine Biotechnology*, New York: John Wiley & Sons. https://doi.org/10.1002/9781119143802.ch36
36. Abdel-Rahman RM, Hrdina R, Abdel-Mohsen AM, et al. (2015) Chitin and chitosan from Brazilian Atlantic Coast: Isolation, characterization and antibacterial activity. *Int J Bio Macromolecules* 80: 107–120. https://doi.org/10.1016/j.ijbiomac.2015.06.027
37. de Andrade SMB, Ladchumananandasivam R, da Rocha BG, et al. (2012) The use of exoskeletons of shrimp (Litopenaeus vanammei) and crab (Ucides cordatus) for the extraction of chitosan and production of nanomembrane. *Mat Sci Appl* 3: 495–508. http://dx.doi.org/10.4236/msa.2012.37070
38. Zhao D, Huang WC, Guo N, et al. (2019) Two-step separation of chitin from shrimp shells using citric acid and deep eutectic solvents with the assistance of microwave. *Polymer* 11: 409. https://doi.org/10.3390/polym11030409
39. Eddya M, Tbib B, Khalil EH (2020) A comparison of chitosan properties after extraction from shrimp shells by diluted and concentrated acids. *Heliyon* 6: e03486. https://doi.org/10.1016/j.heliyon.2020.e03486
40. Zouaoui F, Bourouina-Bacha S, Bourouina M, et al. (2020) Electrochemical sensors based on molecularly imprinted chitosan: A review. *TrAC Trends Analyt Chem* 130: 115982. https://doi.org/10.1016/j.trac.2020.115982
41. Mohammadkhani G, Kumar Ramamoorthy S, Adolfsson KH, et al. (2021) New solvent and coagulating agent for development of chitosan fibers by wet spinning. *Polymer* 13: 2121. https://doi.org/10.3390/polym13132121
42. Tran KM, Do DP, Ta Thi KH, et al. (2019) Influence of top electrode on resistive switching effect of chitosan thin films. *J Mat Res* 34: 3899–3906. https://doi.org/10.1557/jmr.2019.353

43. Zamli MI, Ahmad FB, Akmal MHM (2021) Extraction of microbial chitosan for piezoelectric application. *IOP Conf Ser: Mat Sci Eng* 1045: 012037. https://doi.org/10.1088/1757-899X/1045/1/012037
44. Qiao C, Ma X, Wang X, et al. (2021) Structure and properties of chitosan films: Effect of the type of solvent acid. *Lwt* 135: 109984. https://doi.org/10.1016/j.lwt.2020.109984
45. Baniasadi M, Xu Z, Cai J, et al. (2017) Correlation of annealing temperature, morphology, and electro-mechanical properties of electrospun piezoelectric nanofibers. *Polymer* 127: 192–202. https://doi.org/10.1016/j.polymer.2017.08.053
46. Melro E, Antunes FE, da Silva GJ, et al. (2020) Chitosan films in food applications. Tuning film properties by changing acidic dissolution conditions. *Polymer* 13: 1–12. https://doi.org/10.3390/polym13010001
47. Akmal MM, Warikh ARM, Azlan UAA, et al. (2018) Optimizing the processing conditions of sodium potassium niobate thin films prepared by sol-gel spin coating technique. *Ceram Int* 44: 317–325. https://doi.org/10.1016/j.ceramint.2017.09.175
48. Xu TB (2016) Energy harvesting using piezoelectric materials in aerospace structures, In: Yuan FG, *Structural Health Monitoring (SHM) in Aerospace Structures*, Cambridge: Woodhead Publishing, 175–212. https://doi.org/10.1016/B978-0-08-100148-6.00007-X
49. Wittinanon T, Rianyoi R, Chaipanich A (2021) Electromechanical properties of barium titanate-polyvinylidene fluoride cement-based composites. *Cons Build Mat* 299: 123908. https://doi.org/10.1016/j.conbuildmat.2021.123908
50. Zu H, Wu H, Wang QM (2016) High-temperature piezoelectric crystals for acoustic wave sensor applications. *IEEE Trans Ultrason Eng* 63: 486–505. https://doi.org/10.1109/TUFFC.2016.2527599
51. Krishnaveni B, Ragunathan R (2015) Extraction and characterization of chitin and chitosan from f. Solani cbnr bkrr, synthesis of their bionanocomposites and study of their productive application. *J Pharmac Sci Res* 7: 197–205.
52. Eurofins Medical Device Testing (2018) Biological evaluation of medical devices as an essential part of the risk management process: Updates and challenges of ISO 10993-1: 2018.

AIMS Press

© 2026 the Author(s), licensee AIMS Press. This is an open access article distributed under the terms of the Creative Commons Attribution License (https://creativecommons.org/licenses/by/4.0)